

# Ultrafast manipulation of electron spins in a double quantum dot device: A real-time numerical and analytical study

Gianluca Stefanucci,<sup>1,2,3,\*</sup> Enrico Perfetto,<sup>3,4</sup> and Michele Cini<sup>1,3</sup><sup>1</sup>*Dipartimento di Fisica, Università di Roma Tor Vergata, Via della Ricerca Scientifica 1, I-00133 Rome, Italy*<sup>2</sup>*European Theoretical Spectroscopy Facility (ETSF)*<sup>3</sup>*Laboratori Nazionali di Frascati, Istituto Nazionale di Fisica Nucleare, Via Enrico Fermi 40, 00044 Frascati, Italy*<sup>4</sup>*Dipartimento di Scienza dei Materiali, Università di Milano-Bicocca, Via Cozzi 53, 20125 Milano, Italy*

(Received 26 May 2008; revised manuscript received 21 July 2008; published 20 August 2008)

We consider a double single-level quantum dot system with two embedded and nonaligned spin impurities to manipulate the magnitude and polarization of the electron-spin density. The device is attached to semi-infinite one-dimensional leads which are treated exactly. We provide a real-time description of the electron-spin dynamics when a sequence of ultrafast voltage pulses acts on the device. The numerical simulations are carried out using a spin-generalized modified version of a recently proposed algorithm for the time propagation of open systems [Kurth *et al.*, Phys. Rev. B **72**, 035308 (2005)]. Time-dependent spin accumulations and spin currents are calculated during the entire operating regime, which includes spin-injection and read-out processes. The full knowledge of the electron dynamics allows us to engineer the transient responses and improve the device performance. An approximate rate equation for the electron spin is also derived and used to discuss the numerical results.

DOI: [10.1103/PhysRevB.78.075425](https://doi.org/10.1103/PhysRevB.78.075425)

PACS number(s): 73.63.-b, 72.25.-b, 85.75.Mm

## I. INTRODUCTION

The ability of controlling magnitude and orientation of electron-spin densities in integrated molecules and quantum dots (QDs) is of utmost importance to bring quantum computation closer to real life.<sup>1-3</sup> The microscopic description of nanoscale spin devices, e.g., the two quantum-bit gate envisaged by Loss and Di Vincenzo,<sup>4</sup> constitutes a challenging problem in the theory of open systems far from a steady state. Research activities in the emerging field of spin-dependent transport<sup>5</sup> have mainly focused on steady-state properties. Only very recently the transient dynamics of spin-polarized currents through QDs has attracted some attention<sup>6-11</sup> partly due to experimental advances in manipulating electronic densities with ultrafast voltage pulses.<sup>12-18</sup> This paper goes in the same direction and wants to be a further step toward the bridging of spin-dependent transport and fundamental quantum computation. We perform time-dependent simulations of the charge and spin dynamics of a nanoscale device in contact with one-dimensional leads. The semi-infinite leads are treated *exactly*. The results are analyzed within the framework of nonequilibrium Green's functions.

We consider a double QD device to manipulate the spin orientation of spin-polarized electrons. Both quantum dots contain a static spin impurity with which the electron spin is coupled. Possible experimental realizations of such systems are oxygen vacancies on partially oxidized Si(111) surfaces<sup>19</sup> or iron atoms on Si(111) surfaces.<sup>20</sup> The exchange coupling constant is much larger than experimentally accessible Larmor frequencies, a feature that renders the spin impurity a potentially ultrafast mean to rotate the electron spin.<sup>21,22</sup> Model systems of quantum transport through magnetic QDs have been previously used to study the conductance oscillations of a local nuclear spin in a magnetic field,<sup>23</sup> the gauge-invariant nature of the charge and spin conductances,<sup>24</sup> the

spin-interference and Aharonov-Bohm oscillations in a quantum ring with embedded magnetic impurities,<sup>25-27</sup> and the effects of the entanglement of two spin impurities on the conductance.<sup>28,29</sup>

In this paper we focus on the short-time response of the system when subjected to a sequence of voltage pulses as illustrated in Fig. 1. The injection of spin-polarized electrons from the left lead to the first QD (QD1) is followed by a rotation of the electron spin in QD1. Afterward the electron spin is transferred from QD1 to the second QD (QD2) and its polarization is maintained parallel/antiparallel to the spin impurity of QD2. Eventually, the electron spin in QD2 is read out by calculating the spin current at the interface with the right lead. We provide a time-dependent description of some crucial processes in the theory of spin transport, namely, the injection of spins from a lead to a QD and the spin dynamics of a double QD system weakly coupled to leads. The results of our analysis include: (1) an overshooting of the spin accumulation during the spin-injection phase, (2) a considerable delay in the spin relaxation for different exchange couplings in QD1 and QD2, and (3) oscillations in the transient regime whose frequency depends on the bandwidth of the leads and, therefore, are absent in the commonly used wide-band limit approximation.

The paper is organized as follows. In Sec. II we present our model system and introduce the basic notation. A set of approximate equations to describe different operating processes are derived in Sec. III. We obtain a rate equation for the electron spin of a QD in contact with an electron reservoir and identify the mechanisms leading to a deterioration of the spin polarization and to a damping of the spin magnitude. This analysis will then be used to optimize the spin injection from one of the leads to one of the QDs. We also investigate the spin transfer between the two QDs for different initial orientations of the electron spin. In Sec. IV we use a spin-generalized modified version of the algorithm of Ref.

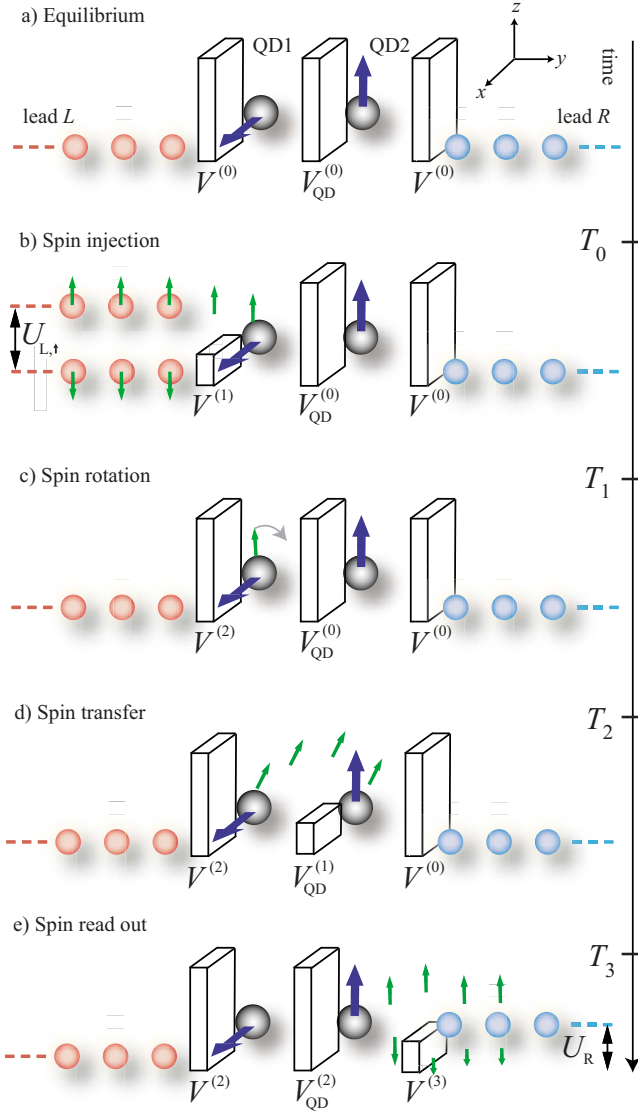


FIG. 1. (Color online) Schematic of the double quantum dot device coupled to leads. At  $t < T_0 = 0$  the system is in equilibrium. At  $T_0$  a spin bias  $U_{L,\uparrow}$  is switched on and, simultaneously, the barrier between QD1 and the left lead is lowered. The injection of spin-up electrons ends at  $T_1$  when the bias is turned off and the barrier is raised. Now the spin in QD1 rotates until  $T_2$  when the barrier between the dots is lowered and the electron spin is transferred from QD1 to QD2. At  $T_3$  the interdot barrier is raised again while the barrier between QD2 and the right lead is lowered. Tuning the electrochemical potential in the right lead  $U_R$  to be in between the two levels of QD2, we measure a large (small) spin current if the electron spin is parallel (antiparallel) to the spin impurity.

30 (see Appendix B) to perform numerical simulations of the microscopic electron dynamics of the double QD system. The results are then interpreted and discussed using the framework developed in Sec. III. In Sec. V we summarize the main findings and discuss future directions.

## II. MODEL SYSTEM

We consider a basic two spin-impurity model consisting of two one-dimensional leads coupled to two single-level

(per spin) QDs. QD1 is connected to the left lead ( $L$ ), QD2 is connected to the right lead ( $R$ ), and a hopping term accounts for tunneling of electrons between QD1 and QD2 (see Fig. 1). The Hamiltonian which describes the system is

$$H = \sum_{\alpha=L,R} H_{\alpha} + H_{\text{QD}} + H_T \quad (1)$$

with  $H_{\alpha}$  the Hamiltonian of the isolated leads,  $H_{\text{QD}}$  the Hamiltonian of the isolated double QD system, and  $H_T$  the tunneling Hamiltonian. The Hamiltonian describing the left ( $L$ ) and right ( $R$ ) leads reads

$$H_{\alpha} = \sum_{\sigma=\uparrow,\downarrow} \sum_{j=0}^{\infty} [V c_{j\alpha,\sigma}^{\dagger} c_{j+1\alpha,\sigma} + V^* c_{j+1\alpha,\sigma}^{\dagger} c_{j\alpha,\sigma}] + \sum_{\sigma=\uparrow,\downarrow} \varepsilon_{\alpha,\sigma}(t) \sum_{j=0}^{\infty} c_{j\alpha,\sigma}^{\dagger} c_{j\alpha,\sigma} \quad (2)$$

with  $\alpha=L,R$ . In Eq. (2) the quantity  $V$  is the hopping integral between nearest-neighbor orbitals and  $\varepsilon_{\alpha,\sigma}(t)$  is the time-dependent on-site energy of lead  $\alpha$  which, in general, can depend on spin. For  $\varepsilon_{\alpha,\sigma}=0$  the energy window of both  $L$  and  $R$  continua is  $(-2|V|, 2|V|)$  and the half-filled system corresponds to a chemical potential  $\mu_{\text{hf}}=0$ . The Hamiltonian of the double QD system reads

$$H_{\text{QD}} = \sum_{i=1}^2 \left[ J_i \vec{S}_i \cdot \sum_{\sigma\sigma'} d_{i,\sigma}^{\dagger} \vec{\sigma}_{\sigma\sigma'} d_{i,\sigma'} + v_i(t) \sum_{\sigma} d_{i,\sigma}^{\dagger} d_{i,\sigma} \right] + \sum_{\sigma} [V_{\text{QD}}(t) d_{1,\sigma}^{\dagger} d_{2,\sigma} + V_{\text{QD}}^*(t) d_{2,\sigma}^{\dagger} d_{1,\sigma}] \quad (3)$$

with  $\vec{S}_i = (\sin \theta_i \cos \phi_i, \sin \theta_i \sin \phi_i, \cos \theta_i)$  the spin of the impurity  $i=1,2$ ,  $J_i > 0$  the corresponding antiferromagnetic exchange coupling, and  $\vec{\sigma} = (\sigma_x, \sigma_y, \sigma_z)$  the Pauli matrices. The interdot tunnel coupling can be tuned by varying the voltage of a gate placed between the dots as shown in Refs. 12 and 16 and can be decreased to values at which the QDs are almost isolated. This is modeled by using time-dependent gate voltages  $v_1(t)$  and  $v_2(t)$  and interdot hopping integral  $V_{\text{QD}}(t)$ . The first term in Eq. (3) is the Hamiltonian of the two isolated QDs and can conveniently be rewritten in matrix form as

$$\sum_{i=1}^2 (d_{i,\uparrow}^{\dagger}, d_{i,\downarrow}^{\dagger}) \begin{pmatrix} v_i + J_i \cos \theta_i & J_i e^{i\phi_i} \sin \theta_i \\ J_i e^{-i\phi_i} \sin \theta_i & v_i - J_i \cos \theta_i \end{pmatrix} \begin{pmatrix} d_{i,\uparrow} \\ d_{i,\downarrow} \end{pmatrix}. \quad (4)$$

From Eq. (4) we see that the isolated QD has two levels at energy  $\varepsilon_{i,\pm} = v_i \pm J_i$ . If  $J_i > |v_i|$  and  $\varepsilon_{\alpha,\sigma}=0$  one level is above  $\mu_{\text{hf}}$  while the other is below.

The double QD system is connected to the left and right leads via the tunneling Hamiltonian

$$H_T = \sum_{\sigma} [V_L(t) d_{1,\sigma}^{\dagger} c_{0L,\sigma} + V_L^*(t) c_{0L,\sigma}^{\dagger} d_{1,\sigma}] + \sum_{\sigma} [V_R(t) d_{2,\sigma}^{\dagger} c_{0R,\sigma} + V_R^*(t) c_{0R,\sigma}^{\dagger} d_{2,\sigma}]. \quad (5)$$

As for the interdot coupling  $V_{\text{QD}}$ , we allow the hopping integrals  $V_L(t)$  and  $V_R(t)$  to be time dependent.

Below we discuss a sequence of operations to manipulate the orientation of the electron spin in QD2 for a fixed orientation of the spin of the injected electrons. Without loss of generality we assume that for negative times ( $t < 0$ ), the whole system is in equilibrium at chemical potential  $\mu$  and inverse temperature  $\beta$  [Fig. 1(a)].<sup>31</sup> The two QDs are initially very weakly coupled to the leads ( $V_\alpha \ll V$ ) and between them,  $V_{\text{QD}} \ll V$ . Furthermore, the two energy levels of both QD1 and QD2 are much larger than the chemical potential, i.e.,  $\varepsilon_{i,\pm} \gg \mu$ , and the population on the dots is practically zero. Starting from this configuration we apply a sequence of four perturbations to: (1) inject spin-up electrons on QD1 [Fig. 1(b)], (2) rotate the electron spin in QD1 [Fig. 1(c)], (3) transfer the electron spin from QD1 to QD2 [Fig. 1(d)], and (4) read out the polarization of the electron spin in QD2 [Fig. 1(e)]. Due to the wide range of possible time-dependent perturbations, we restrict the analysis to piecewise constant (in time) parameters and obtain a set of approximate equations to study the four different processes. This study will then help us in selecting the parameters for target-specific numerical calculations. Full simulations of the entire sequence will be shown in Sec. IV.

### III. THEORETICAL FRAMEWORK

#### A. Spin injection and spin readout

At time  $t=0$  we inject spin-up electrons into QD1 by suddenly switching on a spin bias<sup>32</sup> [ $\varepsilon_{L,\sigma}(t) = \theta(t)U_{L,\sigma}$ ] and reducing the height of the barrier between lead  $L$  and QD1, i.e.,  $V_L(t) = \theta(-t)V^{(0)} + \theta(t)V^{(1)}$ . The injection process terminates by switching off the spin bias and raising the barrier to the equilibrium value  $V^{(0)}$ . There are two different mechanisms which contaminate the spin-up injection with  $x$  and  $y$  components. The first is the spin precession around the spin impurity  $\vec{S}_1$  while the second is the spin-relaxation due to the increased electron hopping  $V_L$ . To tackle this problem we take advantage of the fact that QD1 and QD2 are, during this process, weakly linked and we only consider the electron dynamics on QD1 in contact with the left reservoir, i.e., we approximate  $V_{\text{QD}}=0$ . Using the nonequilibrium Green's function formalism one finds the following equation for the lesser Green's function  $G_{\sigma\sigma'}^<$  on QD1:

$$i \frac{d}{dt} \mathbf{G}^<(t;t) = [\mathbf{H}_{\text{QD1}}, \mathbf{G}^<(t;t)] + \int_0^\infty d\bar{t} \times [\mathbf{\Sigma}_L^<(t;\bar{t}) \mathbf{G}^A(\bar{t};t) + \mathbf{\Sigma}_L^R(t;\bar{t}) \mathbf{G}^<(\bar{t};t) + \text{H.c.}], \quad (6)$$

where we use boldface to indicate  $2 \times 2$  matrices in spin space and the symbol “[,]” denotes a commutator. In the above equation  $\mathbf{H}_{\text{QD1}} = v_1 + J_1 \vec{S}_1 \cdot \vec{\sigma}$  is the one-particle Hamiltonian of the isolated QD1 while  $\mathbf{\Sigma}_L$  is the embedding self-energy of lead  $L$ . We have discarded the integral between 0 and  $-i\beta$  along the imaginary time axis since  $V_L(t < 0) = V^{(0)} \ll V$  and hence  $\mathbf{\Sigma}_L \sim 0$  in equilibrium.<sup>33</sup> The superscripts R/A in  $\mathbf{\Sigma}_L$  and  $\mathbf{G}$  denote retarded/advanced components. The self-energy is diagonal in spin space since there is no spin-flip

hopping between lead  $L$  and QD1. In terms of one-particle eigenstates  $\psi_k(j)$  and eigenenergies  $\varepsilon_k$  of lead  $L$ , one finds for  $t, t' > 0$

$$\Sigma_{L,\sigma\sigma'}^R(t;t') = \delta_{\sigma\sigma'} |V^{(1)}|^2 \int \frac{d\omega}{2\pi} e^{-i(\omega + U_{L,\sigma})(t-t')} \sum_k \frac{|\psi_k(0)|^2}{\omega - \varepsilon_k + i\eta}, \quad (7)$$

$$\Sigma_{L,\sigma\sigma'}^<(t;t') = \delta_{\sigma\sigma'} |V^{(1)}|^2 \int \frac{d\omega}{2\pi} e^{-i(\omega + U_{L,\sigma})(t-t')} i f(\omega) \times 2\pi \sum_k |\psi_k(0)|^2 \delta(\omega - \varepsilon_k). \quad (8)$$

At low temperatures and low biases, only frequencies close to the Fermi energy  $\varepsilon_F$  are probed. Using the wide-band limit (WBL) approximation, i.e.,

$$\sum_k |\psi_k(0)|^2 \delta(\omega - \varepsilon_k) \sim \rho_F \quad (9)$$

with  $\rho_F = \rho(\varepsilon_F)$  the local density of states at the interface, we can approximate Eqs. (7) and (8) as

$$\Sigma_{L,\sigma\sigma'}^R(t;t') = -\frac{i}{2} \delta_{\sigma\sigma'} \Gamma \delta(t-t'), \quad (10)$$

$$\Sigma_{L,\sigma\sigma'}^<(t;t') = i \delta_{\sigma\sigma'} \Gamma \int \frac{d\omega}{2\pi} e^{-i(\omega + U_{L,\sigma})(t-t')} f(\omega) \approx -\delta_{\sigma\sigma'} \frac{\Gamma}{2\pi} e^{-i\varepsilon_{F,\sigma}(t-t')} \left[ \frac{1}{t-t'} - i\pi \delta(t-t') \right], \quad (11)$$

with  $\Gamma = 2\pi |V^{(1)}|^2 \rho_F$  and  $\varepsilon_{F,\sigma} = \varepsilon_F + U_{L,\sigma}$ . In Eq. (11) we have further approximated  $\Sigma_L^<$  with its expression at zero temperature.

Inserting these results into Eq. (6) one obtains

$$i \frac{d}{dt} \mathbf{G}^<(t;t) = [\mathbf{H}_{\text{QD1}}, \mathbf{G}^<(t;t)] - \frac{i}{2} \{ \mathbf{\Gamma}, \mathbf{G}^<(t;t) \} - \mathbf{\Gamma} - \left[ \frac{\mathbf{\Gamma}}{2\pi} \int_0^t d\bar{t} \frac{\exp[-i\varepsilon_F(t-\bar{t})]}{t-\bar{t}} \mathbf{G}^A(\bar{t};t) + \text{H.c.} \right], \quad (12)$$

where the symbol “{,}” denotes the anticommutator and the matrices are  $[\mathbf{\Gamma}]_{\sigma\sigma'} = \delta_{\sigma\sigma'} \Gamma$  and  $[\mathbf{\varepsilon}_F]_{\sigma\sigma'} = \delta_{\sigma\sigma'} \varepsilon_{F,\sigma}$ . From Eq. (12) we can extract a rate equation for the electron spin

$$\vec{S}_{1,el}(t) \equiv -\frac{i}{2} \text{Tr}[\mathbf{G}^<(t;t) \vec{\sigma}] \quad (13)$$

on QD1. In the WBL approximation the advanced Green's function reads

$$\mathbf{G}^A(\bar{t};t) = i\theta(-\Delta t) \exp \left[ -i \left( \mathbf{H}_{\text{QD1}} + \frac{i}{2} \mathbf{\Gamma} \right) \Delta t \right] = i\theta(-\Delta t) e^{-i(v_1 + \frac{i}{2}\Gamma)\Delta t} [\cos(J_1 \Delta t) - i \sin(J_1 \Delta t) \vec{S}_1 \cdot \vec{\sigma}], \quad (14)$$

with  $\Delta t \equiv \bar{t} - t$ . Substituting this result into Eq. (12), multiplying with  $\vec{\sigma}$ , and tracing over the spin indices we find

$$\begin{aligned} \frac{d}{dt} \vec{S}_{1,el} &= J_1 (\vec{S}_1 \wedge \vec{S}_{1,el}) - \frac{\Gamma}{2} \vec{S}_{1,el} - \frac{\Gamma}{\pi} \\ &\times \int_0^t \frac{d\bar{t}}{\Delta t} e^{\frac{\Gamma}{2}\Delta t} \cos((\varepsilon_+ - v_1)\Delta t) \\ &\times [\cos(\varepsilon_- \Delta t) \sin(J_1 \Delta t) \vec{S}_1 - \sin(\varepsilon_- \Delta t) \\ &\times \{\cos(J_1 \Delta t) \hat{z} - \sin(J_1 \Delta t) \hat{z} \wedge \vec{S}_1\}], \end{aligned} \quad (15)$$

with  $\hat{z}$  the unit vector in the  $z$  direction and  $\varepsilon_{\pm} = \varepsilon_{F,\uparrow} \pm \varepsilon_{F,\downarrow}$ . It is instructive to expand the right-hand side in powers of  $t$ . To first order in  $t$  one finds a simplified rate equation for the electron spin

$$\frac{d}{dt} \vec{S}_{1,el} = J_1 (\vec{S}_1 \wedge \vec{S}_{1,el}) - \frac{\Gamma}{2} \vec{S}_{1,el} + \frac{t}{\pi} (\Gamma \varepsilon_- \hat{z} - J_1 \Gamma \vec{S}_1), \quad (16)$$

which is reliable for times  $t^{-1} \geq \max[\varepsilon_-, J_1]/2\pi$ . From the above equation we can identify four different contributions. The term proportional to  $\hat{z}$  is the spin-injection term and is responsible for an increase in the electron spin along the  $z$  direction. Such increase is quadratic in time and faster as the difference  $\varepsilon_- = U_{L,\uparrow} - U_{L,\downarrow}$  becomes larger. The first and the last terms are responsible for a deterioration of the spin direction due to spin precession (first term) and spin relaxation (last term). The latter drives the electron spin toward a configuration antiparallel to the spin impurity  $\vec{S}_1$ . Finally, the second term is responsible for an overall damping of the spin magnitude. Going beyond the first order in  $t$  [see Eq. (15)], one observes the appearance of a new relaxation direction, that is,  $\hat{z} \wedge \vec{S}_1$ . This latter result is completely general as it is only dictated by the symmetry of the system.

We wish to emphasize that the rate Eq. (15) has been derived under the sole assumption that QD1 is initially isolated and then contacted with lead  $L$ . This is the same situation occurring in the spin read-out phase when the barrier between the weakly coupled QD2 and lead  $R$  is lowered. Thus, the rate equation for  $\vec{S}_{2,el}$  during the read-out phase is identical to Eq. (15) for  $\vec{S}_{1,el}$  even though the parameters are different and, more importantly, different initial conditions must be imposed.

### B. Spin rotation and spin transfer

After a time  $T_1$  the spin bias is switched off and the hopping  $V_L$  is again reduced to values much smaller than  $V$ . In this phase QD1 is well isolated and the electron spin precesses around the spin impurity  $\vec{S}_1$  according to

$$\frac{d}{dt} \vec{S}_{1,el} = J_1 (\vec{S}_1 \wedge \vec{S}_{1,el}), \quad t > T_1. \quad (17)$$

Let us now specialize to the situation illustrated in Fig. 1 with  $\vec{S}_1$  oriented along the positive  $x$  axis and  $\vec{S}_2$  along the positive  $z$  axis. We recall that the Fermi energy is much

smaller than the energy levels of the two isolated QDs and hence that the equilibrium electron density is vanishingly small. For  $J_1 \gg \varepsilon_-$  [see Eq. (16)], we expect an efficient injection of spin-up electrons in QD1 and for  $J_1 \gg \Gamma$  a major contamination along the  $y$  direction. This implies that the electron spin  $\vec{S}_{1,el}(T_1)$  has a small  $x$  component at the end of the spin-injection process. Since  $\vec{S}_1$  is parallel to the  $x$  axis,  $\vec{S}_{1,el}(t)$  rotates in the  $yz$  plane for  $t > T_1$ . We let the system evolve until a time  $T_2 > T_1$  and we approximate  $\vec{S}_{1,el}(T_2) = (0, S_{1,el}^y(T_2), S_{1,el}^z(T_2))$  on the  $yz$  plane and  $\vec{S}_{2,el}(T_2) = 0$  (this latter approximation comes from the fact that  $V_{\text{QD}}$  and  $V_R$  are both much smaller than  $V$  for  $t < T_2$ ).

At  $t = T_2$  we transfer the electron spin by lowering the barrier between QD1 and QD2. This corresponds to an increase in the interdot hopping  $V_{\text{QD}}$ . Letting  $|\Phi(T_2)\rangle$  be the evolved many-particle state of the entire system at  $t = T_2$ , the density matrix  $\rho$  of the double quantum dot system has matrix elements  $[\rho]_{i\sigma, j\sigma'} = \langle \Phi(T_2) | d_{j,\sigma'}^\dagger d_{i,\sigma} | \Phi(T_2) \rangle$ . It is convenient to introduce the notation  $1 = (1, \uparrow)$ ,  $2 = (1, \downarrow)$ ,  $3 = (2, \uparrow)$ , and  $4 = (2, \downarrow)$  for the collective index  $(i, \sigma)$ . The density matrix is then represented by the following  $4 \times 4$  matrix:

$$\rho = 2S_{1,el}(T_2) \begin{pmatrix} \cos^2 \theta & -\frac{i}{2} \sin 2\theta & 0 & 0 \\ \frac{i}{2} \sin 2\theta & \sin^2 \theta & 0 & 0 \\ 0 & 0 & 0 & 0 \\ 0 & 0 & 0 & 0 \end{pmatrix}, \quad (18)$$

with  $\sin 2\theta = S_{1,el}^y(T_2)/S_{1,el}(T_2)$ ,  $\cos 2\theta = S_{1,el}^z(T_2)/S_{1,el}(T_2)$ , and  $S_{1,el} = \sqrt{\vec{S}_{1,el} \cdot \vec{S}_{1,el}}$  is the spin magnitude. We are interested in how to choose the angle  $\theta$  in order to maximize the electron spin of QD2 along the  $z$  direction (parallel/antiparallel to the spin impurity  $\vec{S}_2$ ). For simplicity we take the gate voltages  $v_1 = 0$  and  $v_2 = 0$ . Then the isolated double QD system is described by the  $4 \times 4$  Hamiltonian matrix

$$\mathbf{H}_{\text{QD}} = \begin{pmatrix} J_1 \sigma_x & V_{\text{QD}} \mathbf{1}_2 \\ V_{\text{QD}} \mathbf{1}_2 & J_2 \sigma_z \end{pmatrix}, \quad (19)$$

with  $\mathbf{1}_2$  the  $2 \times 2$  identity matrix. In terms of  $\rho$  and  $\mathbf{H}_{\text{QD}}$ , the  $z$  component  $S_{2,el}^z$  of the electron spin on QD2 is given by

$$S_{2,el}^z(t + T_2) = \frac{1}{2} \text{Tr}[\Sigma_2^z \exp(i\mathbf{H}_{\text{QD}}t) \rho \exp(-i\mathbf{H}_{\text{QD}}t)], \quad (20)$$

with the spin operator of QD2

$$\Sigma_2^z = \begin{pmatrix} \mathbf{0}_2 & \mathbf{0}_2 \\ \mathbf{0}_2 & \sigma_z \end{pmatrix}, \quad (21)$$

and  $\mathbf{0}_2$  the  $2 \times 2$  null matrix. Substituting  $\rho$  from Eq. (18) we find

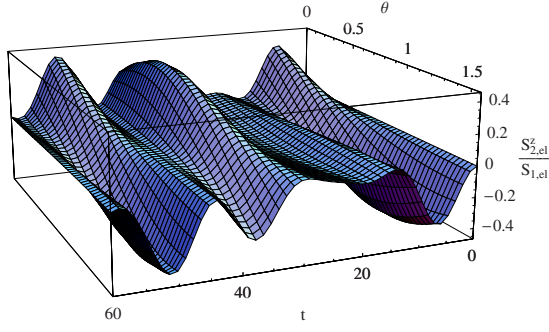


FIG. 2. (Color online) Ratio  $S_{2,el}^z(t+T_2)/S_{1,el}(T_2)$  versus time  $t$  and initial polarization  $\theta$  for  $J_1=J_2=0.1$  and  $V_{QD}=0.2$ .

$$\frac{S_{2,el}^z(t+T_2)}{S_{1,el}(T_2)} = \frac{i}{2} \sin 2\theta [\Sigma_2^z(t)]_{1,2} - [\Sigma_2^z(t)]_{2,1} + \cos^2 \theta [\Sigma_2^z(t)]_{1,1} + \sin^2 \theta [\Sigma_2^z(t)]_{2,2}, \quad (22)$$

where we have defined the spin operator in the Heisenberg representation

$$\Sigma_2^z(t) \equiv \exp(-i\mathbf{H}_{QD}t)\Sigma_2^z \exp(i\mathbf{H}_{QD}t). \quad (23)$$

It is easy to prove that the function  $O(t) \equiv \frac{i}{2}([\Sigma_2^z(t)]_{1,2} - [\Sigma_2^z(t)]_{2,1})$  is an odd function of time while  $[\Sigma_2^z(t)]_{1,1}$  and  $[\Sigma_2^z(t)]_{2,2}$  are even functions of time. In Appendix A we further prove that

$$E(t) \equiv [\Sigma_2^z(t)]_{1,1} = -[\Sigma_2^z(t)]_{2,2}, \quad (24)$$

which leads to the simple formula

$$\begin{aligned} S_{2,el}^z(t+T_2) &= S_{1,el}(T_2)[O(t)\sin 2\theta + E(t)\cos 2\theta] \\ &= O(t)S_{1,el}^y + E(t)S_{1,el}^z. \end{aligned} \quad (25)$$

The function  $E(t)$  can be written as a linear combination of the cosine functions  $\cos(\omega_{\mu\nu}t)$  while  $O(t)$  as a linear combination of the sine functions  $\sin(\omega_{\mu\nu}t)$ , where  $\omega_{\mu\nu} = \varepsilon_\mu - \varepsilon_\nu$  is the difference between two eigenvalues of  $\mathbf{H}_{QD}$ . The eigenvalues  $\varepsilon_\mu$ , where  $\mu=1, \dots, 4$ , can be calculated analytically and read

$$\varepsilon_\mu = \pm \sqrt{\frac{J_+^2 + 2V_{QD}^2 \pm \sqrt{J_-^4 + 4J_+^2V_{QD}^2}}{2}}, \quad (26)$$

with  $J_\pm^2 = J_1^2 \pm J_2^2$ .

As an example, in Fig. 2 we plot the ratio  $S_{2,el}^z(t+T_2)/S_{1,el}(T_2)$  as a function of time  $t$  and initial polarization  $\theta$  for  $J_1=J_2=0.1$  and  $V_{QD}=0.2$ . We notice that for most polarizations,  $S_{2,el}^z(t+T_2)$  remains smaller than 0.2. Only for some special value of  $\theta$  the  $z$  component of the spin in QD2 reaches a value larger than 0.4. This means that the maximum efficiency in transferring an electron spin polarized in the  $yz$  plane from QD1 to QD2 with final polarization along the positive  $z$  axis is about 80%–90%.

All above processes can be numerically simulated without resorting to any of the approximations employed in this section. This allows for a more quantitative investigation of the device performance and it will be the topic of Sec. IV.

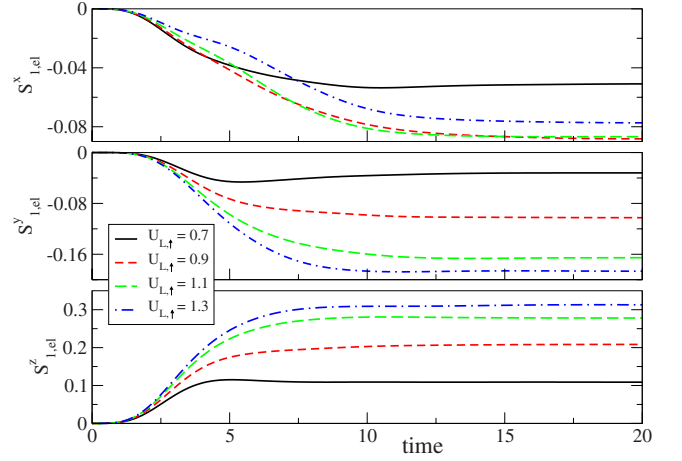


FIG. 3. (Color online) The three components of the electron spin in QD1 versus time for a sudden change in the hopping  $V_L$  from  $V^{(0)}=0.01$  to  $V^{(1)}=0.5$  and a simultaneous sudden switching of the spin bias  $U_{L,\uparrow}=0.7, 0.9, 1.1, 1.3$ . The equilibrium parameters are  $J_1=J_2=0.1$  and  $V_L=V_R=V_{QD}=V^{(0)}$  and the Fermi energy is  $\varepsilon_F=-0.96$ .

#### IV. NUMERICAL SIMULATIONS AND DISCUSSION

In this section we use a modified version of the algorithm proposed in Ref. 30 to propagate in time finite systems in contact with infinitely long leads (see Appendix B) and investigate the microscopic dynamics of the spin injection, the spin accumulation, as well as the spin rotation of conducting electrons scattering against the double QD device of Eq. (3). In the following analysis energies are measured in units of  $V$ , times in units of  $\hbar/V$ , spins in units of  $\hbar$ , and currents in units of  $eV/\hbar$  with  $e$  as the electron charge. The full Hamiltonian is time independent for negative times and the system is in equilibrium at zero temperature and Fermi energy  $\varepsilon_F$ .<sup>31</sup> We start by considering two identical QDs with exchange coupling  $J_1=J_2=0.1$  and gate potential  $v_1=v_2=0$  weakly coupled to the left and right leads [ $V_L=V_R=V^{(0)}=0.01$ ] and with interdot hopping  $V_{QD}=0.01$ . Choosing  $V \sim 100$  meV the exchange couplings  $J_1, J_2 \sim 10$  meV lie in the physical parameter range<sup>22</sup> and the corresponding time unit is  $\hbar/V \sim 100$  fs, which is appropriate to study ultrafast dynamics.<sup>34,35</sup> The impurity spin  $\vec{S}_1$  of QD1 is oriented along the positive  $x$  axis while  $\vec{S}_2$  is oriented along the positive  $z$  axis. The on-site energies of the leads  $\varepsilon_{\alpha,\sigma}$  are initially all zero.

##### A. Spin injection

At time  $t=0$  we switch on a spin bias  $\varepsilon_{L,\uparrow}(t) = \theta(t)U_{L,\uparrow}$  in lead  $L$  for spin-up electrons ( $U_{L,\downarrow}=0$ ) and increase the hopping  $V_L$  from  $V^{(0)}$  to  $V^{(1)}$ .

In Fig. 3 we study the spin-injection process when the Fermi energy is  $\varepsilon_F=-0.96$  (which corresponds to an initial electron occupation on QD1 of the order of  $10^{-5}$ ) and the hopping between  $L$  and QD1 at positive times is  $V^{(1)}=0.5$ . We calculate the time-dependent expectation value of the spin of the conducting electrons  $\vec{S}_{1,el}$  on QD1 for different

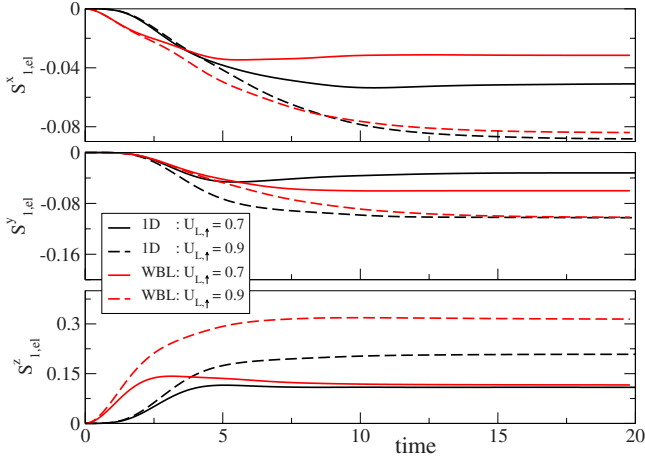


FIG. 4. (Color online) Comparison between the results obtained with one-dimensional (1D) leads and WBL leads for the electron spin in QD1 and  $U_{L,\uparrow}=0.7, 0.9$ . The other parameters are the same as in Fig. 3.

biases  $U_{L,\uparrow}$ . Since  $U_{L,\uparrow} \sim 1 > J_1$ , the rate Eq. (16) is reliable for times  $t \leq 2\pi/U_{L,\uparrow} \sim 2\pi$ . In this time window we observe that the  $z$  component  $S_{1,el}^z$  increases quadratically in time and that the rate is larger, the larger the spin bias  $U_{L,\uparrow}$  is, in agreement with Eq. (16) (we recall that in this case,  $\varepsilon_- = U_{L,\uparrow}$ ). The  $y$  component  $S_{1,el}^y$  has a trend similar to  $S_{1,el}^z$  but the transient is even smoother. This can be explained by observing that as the spin-up electrons enter QD1 they undergo a spin rotation due to the spin impurity oriented along the positive  $x$  axis. Taking into account that for small  $t$  we have  $S_{1,el}^z \sim t^2$ , from Eq. (16) we see that  $S_{1,el}^y \sim J_1 t^3$ . As the  $z$  component also the  $x$  component  $S_{1,el}^x$  grows quadratically in time. From Eq. (16) one finds  $S_{1,el}^x(t)/S_{1,el}^z(t) \sim \varepsilon_-/J_1$ , meaning that to minimize the contamination of spin-up electrons with an  $x$  component it must be  $\varepsilon_-/J_1 > 1$ .

We wish to observe that at intermediate biases  $U_{L,\uparrow}$ , the numerical results agree with the rate Eq. (15) only qualitatively. The comparison between the time evolutions of the electron spin in QD1 for  $U_{L,\uparrow}=0.7, 0.9$  as obtained with one-dimensional leads and with leads treated in the WBL approximation is shown in Fig. 4.

In Fig. 5 we fix the bias for spin-up electrons to be  $U_{L,\uparrow}=1.3$  and analyze the spin dynamics on QD1 for different values of  $V^{(1)}$ . We first observe that the transient time decreases by increasing  $V^{(1)}$  and hence  $\Gamma$ . This is easily understood by noticing that the second term in Eq. (15) yields an exponential damping of the spin oscillations. The spin oscillations can be observed in the  $y$  and  $z$  components and are due to the spin precession around the spin impurity  $\vec{S}_1$ . The period of the oscillation is  $T = \pi/J_1$  and is independent of  $V^{(1)}$ , as it should. It is also interesting to observe that for small times,  $S_{1,el}^z$  overshoots its steady value and hence more efficient spin injections may be achieved by properly engineering the transient response. In our case, for an efficient spin-up injection, only the ratios  $r_{xy} = |S_{1,el}^x/S_{1,el}^y|$  and  $r_{xz} = |S_{1,el}^x/S_{1,el}^z|$  must be small at the end of the process since the  $y$  component can be reduced to zero in the second phase when  $V_L \ll V$  and  $\vec{S}_{1,el}$  can precess around the spin impurity.

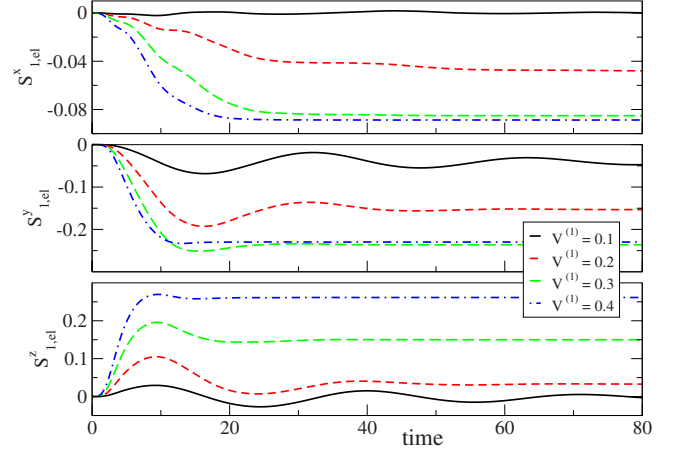


FIG. 5. (Color online) The three components of the electron spin in QD1 versus time for a sudden switching of the spin bias  $U_{L,\uparrow}=1.3$  and a simultaneous sudden change of the hopping  $V_L$  from  $V^{(0)}=0.01$  to  $V^{(1)}=0.1, 0.2, 0.3, 0.4$ . The other parameters are the same as in Fig. 3.

From Fig. 5 we find that for  $V^{(1)}=0.2$  and at  $t \sim 10$ , the ratios are  $r_{xy} \sim 0.1$  and  $r_{xz} \sim 0.12$  while at the steady state  $r_{xy} \sim 0.31$  and  $r_{xz} \sim 1.43$ .

## B. Spin rotation

The injection process terminates after some time  $T_1$  by switching the spin bias off and raising back the barrier between QD1 and the left lead, i.e.,  $V_L(t) = \theta(-t)V^{(0)} + \theta(t)\theta(T_1-t)V^{(1)} + \theta(t-T_1)V^{(2)}$ . During the second phase QD1 is weakly coupled to the environment and the electron spin precesses around  $\vec{S}_1$ . Let us focus on the situation discussed above with  $V^{(1)}=0.2$  and let  $T_1=10$  be the duration of the first phase. In Fig. 6 we study the electron spin on QD1 [Figs. 6(a) and 6(b)] and the densities  $n_{L,\sigma} \equiv \langle c_{0L,\sigma}^\dagger c_{0L,\sigma} \rangle$  on the first site of the left electrode [Fig. 6(c)] for  $V^{(2)}=0.01$ . The contaminating component  $S_{1,el}^x$  ceases to decrease at  $t = T_1$  while the  $y$  and  $z$  components are well described by damped cosine functions with a phase lag of  $\pi/(4J_1)$  [Fig. 6(a)]. Due to the weak contact  $V^{(2)}$  the magnitude  $S_{1,el} = \sqrt{\vec{S}_{1,el} \cdot \vec{S}_{1,el}}$  of the electron spin changes on a time scale much longer than the spin-exchange time scale  $\sim 1/J_1$ . This is shown in Fig. 6(b) where the trajectory of  $\vec{S}_{1,el}$  is projected onto the  $yz$  plane. For times  $t < T_1$ , the trajectory has a large radial component while for  $t > T_1$ , the spin moves along a spiral trajectory. It is also interesting to look at the densities on the nearest-neighbor site of QD1 [Fig. 6(c)]. During the first phase ( $t < T_1$ ) a majority of spin-up electrons are transferred from lead  $L$  to QD1 and, as a consequence,  $n_{L,\uparrow}$  decreases. On the contrary the density  $n_{L,\downarrow}$  increases due to the following two-step mechanism. As the spin-up electrons hop from lead  $L$  to QD1, they undergo a spin rotation and acquire a down component. These electrons have about zero energy and can easily hop to the left lead where the spin-down band is filled up to  $\varepsilon_F + U_{L,\downarrow} = \varepsilon_F = -0.96$ . At the end of the injection process the densities change abruptly and approach their initial value since  $V^{(2)} = V^{(0)}$ . The inset of Fig. 6(c) is a mag-

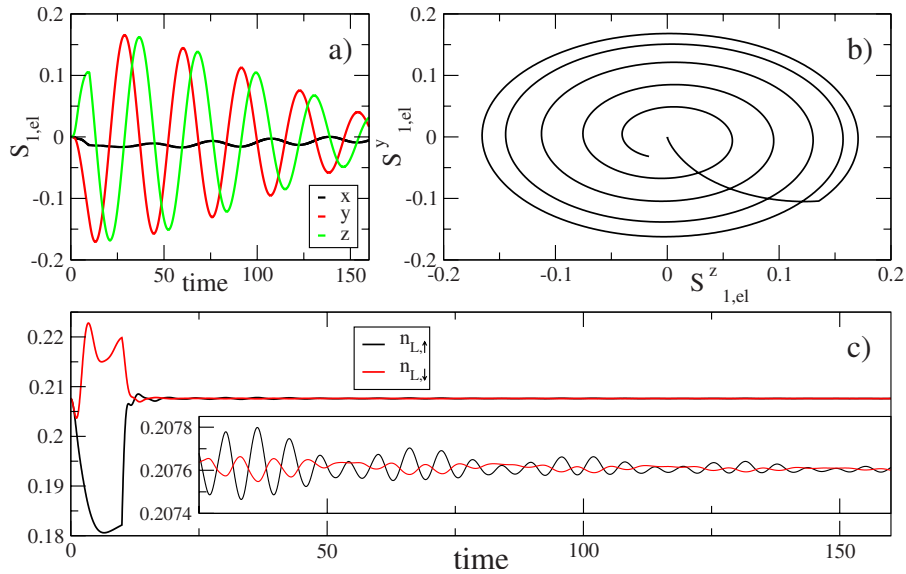


FIG. 6. (Color online) Electron spin in QD1 and electron density at the left interface during the injection phase ( $t < T_1$ ) and the rotation phase ( $t > T_1$ ) when  $T_1 = 10$ . The equilibrium parameters are the same as in Fig. 5, i.e.,  $J_1 = J_2 = 0.1$  and  $V_L = V_R = V_{\text{QD}} = V^{(0)}$  and the Fermi energy is  $\varepsilon_F = -0.96$ . For  $0 < t < T_1$  the system is perturbed by a spin bias  $U_{L,\uparrow} = 1.3$  and a larger hopping  $V_L = V^{(1)} = 0.2$ . At  $t = T_1$  the spin bias is switched off and the hopping  $V_L$  is suddenly changed to  $V^{(2)} = 0.01$ . (a) The three components of  $\vec{S}_{1,el}$ . (b) The trajectory of the projection of  $\vec{S}_{1,el}$  onto the  $yz$  plane. (c) Spin-up and -down densities on the first site of the left lead. The inset is a magnification of both densities  $n_{L,\uparrow}$  and  $n_{L,\downarrow}$  for times  $t > 25$ .

nification of the curves  $n_{L,\uparrow}(t)$  and  $n_{L,\downarrow}(t)$  for  $25 < t < 160$ . A quantum beating in both densities due to the alignment of the spin impurity along the  $x$  axis is clearly visible. In both cases two oscillations with frequency  $|\varepsilon_F \pm J_1| = 0.96 \pm 0.1$  are superimposed to an envelope oscillation of frequency  $2J_1 = 0.2$ .

The spin rotation phase is further investigated in Fig. 7 where we consider the same system as in Fig. 6 except for

the value of the hopping parameter  $V^{(2)} = 0.06$ , which is six times larger [Figs. 7(a) and 7(b)], or the exchange coupling  $J_2 = 0.02$ , which is five times smaller [Figs. 7(c) and 7(d)]. In the first case the  $x$  component remains an order of magnitude smaller than  $S_{1,el}$  [see Fig. 7(a)] and eventually approaches a steady value slightly larger than the initial one (not shown). As in Fig. 6 the electron spin is damped in all three directions but it decays faster. The projection of  $\vec{S}_{1,el}$  onto the  $yz$

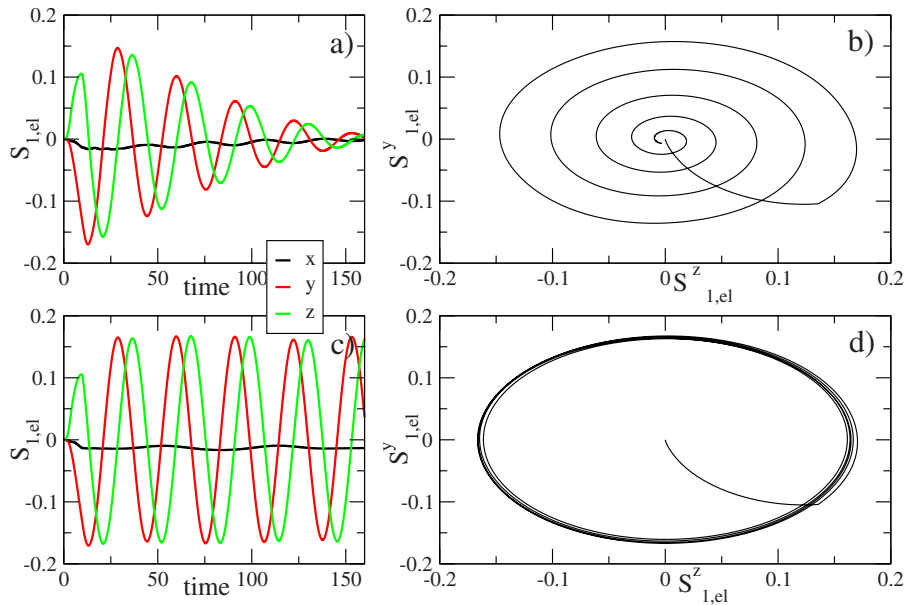


FIG. 7. (Color online) (a) The three components of  $\vec{S}_{1,el}$  and (b) the trajectory of the projection of  $\vec{S}_{1,el}$  onto the  $yz$  plane for the same system as in Fig. 6 except that the hopping parameter  $V^{(2)} = 0.06$  is six times larger. (c) and (d) Same as (a) and (b) but with the equilibrium parameter  $J_2 = 0.02$  and hopping parameter  $V^{(2)} = 0.01$ .

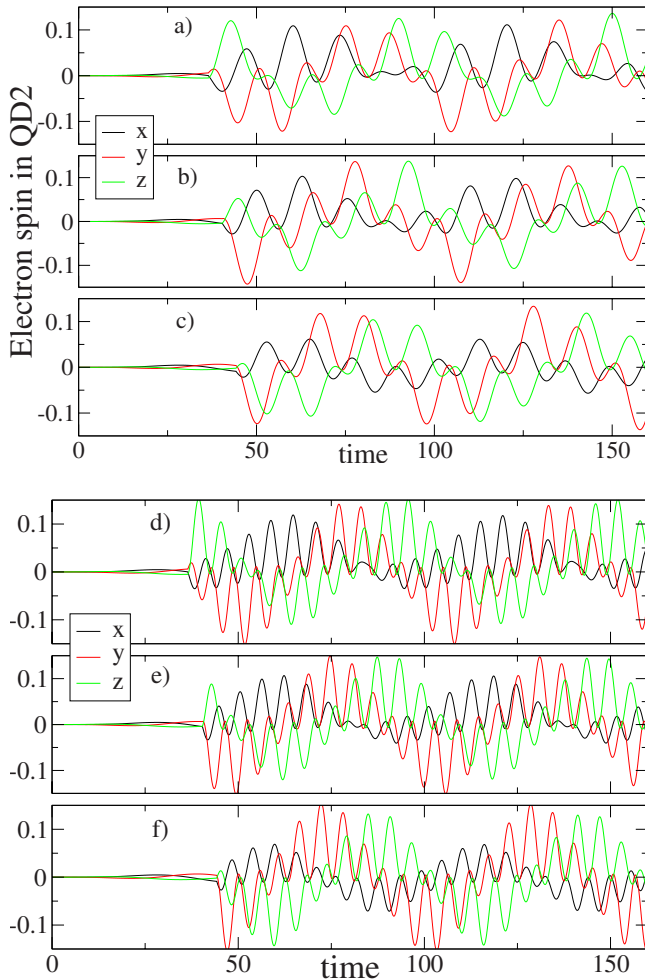


FIG. 8. (Color online) The electron spin  $\vec{S}_{2,el}$  in QD2 before ( $t < T_2$ ) and after ( $t > T_2$ ) the spin transfer phase when the interdot hopping is set to (a)–(c)  $V_{\text{QD}}^{(1)} = 0.2$  and (d)–(f)  $V_{\text{QD}}^{(1)} = 0.5$ . The transfer phase starts at (a) and (d)  $T_2 \sim 36.5$ , (b) and (e)  $T_2 \sim 40.4$ , and (c) and (f)  $T_2 \sim 44.3$ . All parameters before time  $T_2$  are the same as in Fig. 6 except for the exchange coupling  $J_2 = 0.05$ .

plane [Fig. 7(b)] yields a spiral trajectory, which finishes very close to the origin after a time  $t \sim 160$ . On the other hand, for a smaller coupling  $J_2 = J_1/5$ , we do not appreciate any damping within the time propagation window  $t < 160$ . The  $y$  and  $z$  components of  $\vec{S}_{1,el}$  are well described by two undamped cosine functions with a phase lag of  $\pi/(4J_1)$  and an amplitude which is about ten times larger than  $|S_{1,el}^x|$  [see Fig. 7(c)]. In Fig. 7(d) we show the projection of  $\vec{S}_{1,el}$  onto the  $yz$  plane. The reduced damping is a desirable feature and has to be attributed to the mismatch of the energy levels in the two quantum dots:  $\pm J_1$  in QD1 and  $\pm J_2$  in QD2.

### C. Spin transfer

The rotation of the electron spin in QD1 ( $t > T_1$ ) terminates at  $t = T_2 > T_1$  when the barrier between QD1 and QD2 is lowered and, as a consequence, the interdot hopping increases, i.e.,  $V_{\text{QD}} = V_{\text{QD}}^{(0)}\theta(T_2 - t) + V_{\text{QD}}^{(1)}\theta(t - T_2)$ , where  $V_{\text{QD}}^{(0)} = 0.01$ . This is the spin transfer phase. In Fig. 8 we plot the

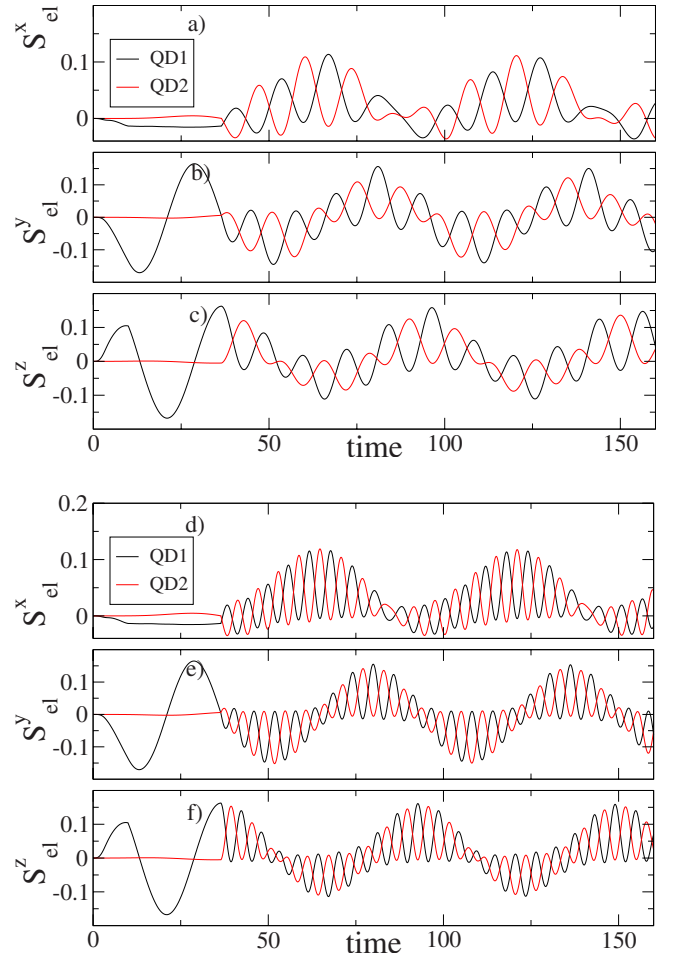


FIG. 9. (Color online) Electron spin in QD1 and QD2 for  $T_2 = 36.5$  and (a)–(c)  $V_{\text{QD}}^{(1)} = 0.2$  and (d)–(f)  $V_{\text{QD}}^{(1)} = 0.5$ . The other parameters are the same as in Fig. 8.

three components of the electron spin in QD2 versus time for  $V_{\text{QD}}^{(1)} = 0.2$  [Figs. 8(a)–8(c)] and  $V_{\text{QD}}^{(1)} = 0.5$  [Figs. 8(d)–8(f)]. For times  $t < T_2$  the system undergoes the same perturbations as in Figs. 6 and 7. Here we have considered an exchange coupling in QD2 of  $J_2 = 0.05$  and a hopping  $V_{\text{QD}}^{(2)} = 0.01$ . The frequency of the oscillations is larger, the larger the interdot coupling is, in agreement with Eq. (26). The efficiency of the transfer has been investigated for different times  $T_2$  at which the electron spin in QD1 is polarized along  $\hat{z}$  [ $T_2 \sim 36.5$ , Figs. 8(a) and 8(d)],  $\frac{1}{\sqrt{2}}(\hat{z} - \hat{y})$  [ $T_2 \sim 40.4$ , Figs. 8(b) and 8(e)], and  $-\hat{y}$  [ $T_2 \sim 44.3$ , Figs. 8(c) and 8(f)]. For our choice of parameters the efficiency is higher if the spin in QD1 is polarized along  $\hat{z}$ .

We also observe that for all three components, the maxima of the electron spin in QD1 correspond to the minima of the electron spin in QD2—see Fig. 9 where we plot  $\vec{S}_{1,el}$  and  $\vec{S}_{2,el}$  at  $T_2 = 36.5$  for  $V_{\text{QD}}^{(1)} = 0.2$  [Figs. 9(a)–9(c)] and  $V_{\text{QD}}^{(1)} = 0.5$  [Figs. 9(d)–9(f)]. From Fig. 8(d) and Figs. 9(d)–9(f) one observes that when  $T_2$  corresponds to the time at which  $\vec{S}_{1,el}(T_2)$  is polarized along  $\hat{z}$ , the maxima of  $S_{2,el}^z$  are close to the zeros of  $S_{2,el}^x$  and  $S_{2,el}^y$ , in agreement with the analysis of Sec. III B. We define the ratio  $r_{\perp} \equiv S_{2,el}^z / \sqrt{(S_{2,el}^x)^2 + (S_{2,el}^y)^2}$ . In the propagation window the

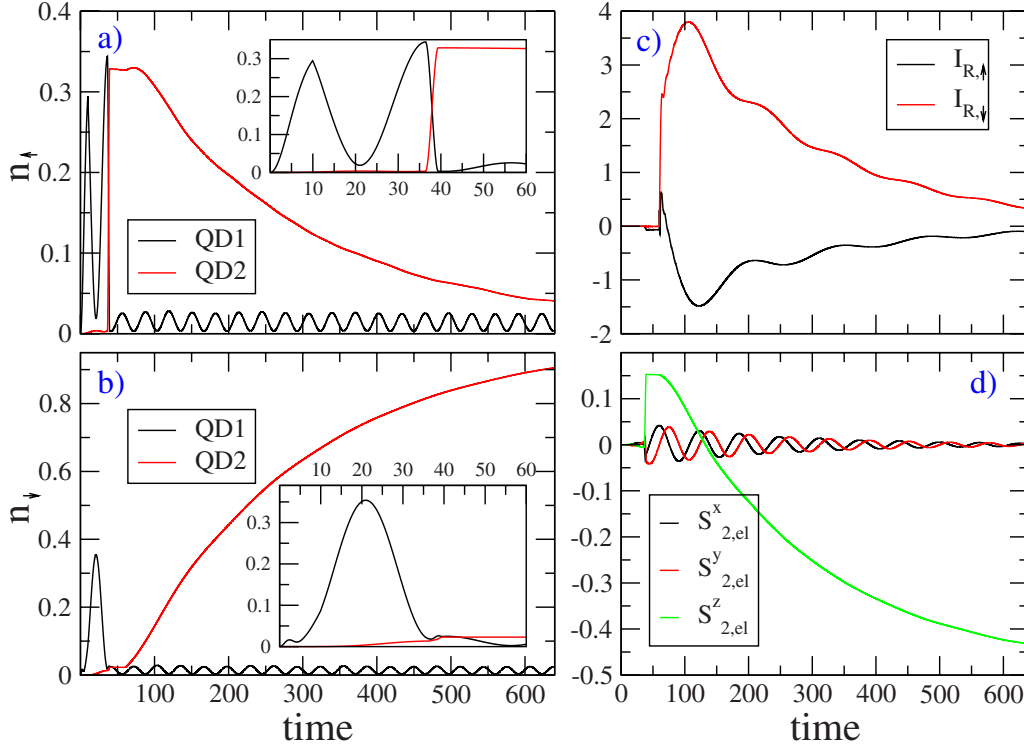


FIG. 10. (Color online) (a) Spin-up density and (b) spin-down density in QD1 and QD2 (the inset shows a magnification of the time window  $0 < t < 60$ ). The spin-polarized current at the right interface  $[I_{R,\sigma}(t)]$  is displayed in (c) in units of  $10^{-3}$  while (d) shows  $\vec{S}_{2,el}(t)$ . For  $t < T_3 = 39.32$  the system parameters and the perturbations are the same as in Fig. 9 with  $V_{\text{QD}}^{(1)} = 0.5$ . For  $t \geq T_3$  the interdot hopping is lowered to the value  $V_{\text{QD}}^{(2)} = 0.001$  and QD2 becomes a well-isolated system. At  $t = 60 > T_3$  the hopping  $V_R(t)$  between QD2 and lead  $R$  is raised to  $V^{(3)} = 0.05$  and, simultaneously, a bias  $U_{R,\uparrow} = U_{R,\downarrow} = 0.96$  is switched on in the right lead. At this time the electrochemical potential in lead  $R$  is  $\mu_R = \varepsilon_F + 0.96 = 0$  and lies in between the two spin levels of QD2.

maxima of  $S_{2,el}^z$  occur at  $t = 39.32$  when  $r_{\perp} \sim 0.28$  and  $S_{2,el}^z = 0.153$ ,  $t = 95.68$  when  $r_{\perp} \sim 0.26$  and  $S_{2,el}^z = 0.152$ , and  $t = 151.96$  when  $r_{\perp} \sim 0.24$  and  $S_{2,el}^z = 0.151$ . Taking into account that  $S_{1,el}^z(T_2) = 0.163$ , the efficiency of the spin transfer can be up to 90%.

#### D. Spin readout

At a time  $t = T_3$  when  $S_{2,el}^z$  has a maximum or a minimum, the interdot hopping is lowered, i.e.,  $V_{\text{QD}}(t) = V_{\text{QD}}^{(0)}\theta(T_2 - t) + V_{\text{QD}}^{(1)}\theta(t - T_2)\theta(T_3 - t) + V_{\text{QD}}^{(2)}\theta(t - T_3)$  with  $V_{\text{QD}}^{(2)} \ll V$ , and the spin transfer phase ends.

In Fig. 10 we consider the same system parameters and perturbations of Fig. 9 (with  $V_{\text{QD}}^{(1)} = 0.5$ ) and fix the time  $T_3 = 39.32$  when  $S_{2,el}^z$  has a maximum. At  $t = T_3$  the interdot hopping is lowered to  $V_{\text{QD}}^{(2)} = 0.001$  and QD2 becomes an almost isolated system. At this stage the density of spin-up and -down electrons in QD2 is practically constant as one can see from the insets of Figs. 10(a) and 10(b). Shortly after  $T_3$  the read-out phase starts. At  $t = 60$  we lower the barrier between QD2 and lead  $R$  and simultaneously switch on a bias  $U_{R,\uparrow} = U_{R,\downarrow} = U_R = 0.96$  in the right lead. The electrochemical potential in lead  $R$  becomes  $\mu_R = \varepsilon_F + U_R = 0$  and lies in between the two energy levels  $\varepsilon_{2,\pm} = \pm J_2 = \pm 0.05$  of the isolated QD2, with the highest level  $\varepsilon_{2,+}$  for spin-up electrons and the lowest level  $\varepsilon_{2,-}$  for spin-down electrons.<sup>36</sup> Spin-up electrons in QD2 have, therefore, energy larger than  $\mu_R$  and tunnel to

the lead  $R$ . As a consequence the spin-up density decreases as one can see in Fig. 10(a). On the contrary, the lowest level  $\varepsilon_{2,-}$  has energy below  $\mu_R$  and a vanishingly small occupation. Spin-down electrons tunnel from lead  $R$  to QD2 and the density of spin-down electrons increases [see Fig. 10(b)]. This charge transfer generates a right-going spin-up current  $I_{R,\uparrow}$  and a left-going spin-down current  $I_{R,\downarrow}$  [see Fig. 10(c)], which results in a large spin current. The spin dynamics in the  $xy$  plane is displayed in Fig. 10(d) where, besides the monotonically decreasing  $z$  component, we plot the  $x$  and  $y$  components of  $\vec{S}_{2,el}$ . Due to the symmetry of the problem,  $S_{2,el}^x$  and  $S_{2,el}^y$  oscillate around zero with an exponentially decreasing amplitude.

The situation corresponding to the antiparallel configuration in QD2 is analyzed in Fig. 11. The difference with the previous case is that we let the electron spin in QD1 rotate until it is polarized along the negative  $z$  axis. The first time  $S_{1,el}^z$  is minimum occurs at  $T_2 = 52.05$  [see insets in Figs. 11(a) and 11(b)]. The spin transfer phase ends at  $T_3 = 54.84$  with an efficiency of about 90%. This can be seen in the inset of Fig. 11(b) where the spin-down density of QD2 swaps with that of QD1 in the time window  $(T_2, T_3)$ . At  $t = T_3$  the system undergoes the same perturbations considered in Fig. 10. Being the spin-up level of QD2 scarcely populated, the change in the spin-up density [Fig. 11(a)] and spin-up current at the right interface [Fig. 11(c)] is very small as compared to the parallel configuration. A small change is observed for the

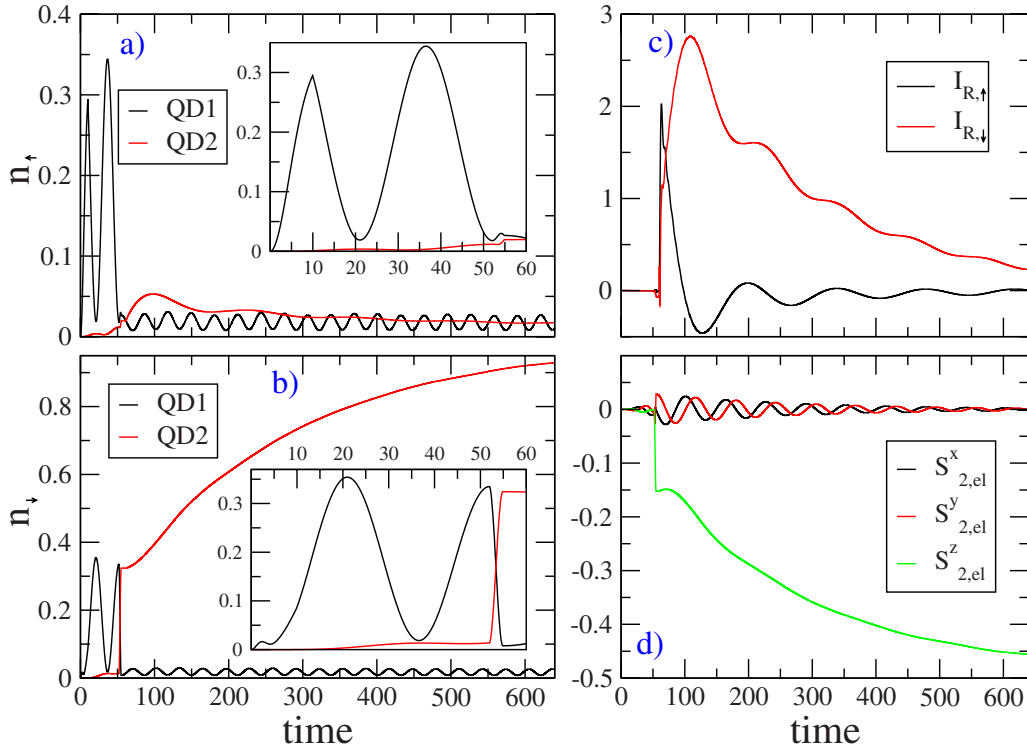


FIG. 11. (Color online) (a) Spin-up density and (b) spin-down density on QD1 and QD2. Spin-polarized current at the right interface ( $I_{R,\sigma}$ ) in units of  $10^{-3}$  (c) and  $\hat{S}_{2,el}^z$  (d). The insets of (a) and (b) show a magnification of the density in the time window  $0 < t < 60$ . Same system parameters and perturbations of Fig. 10 but  $T_2=52.05$  and  $T_3=54.84$ .

spin-down quantities as well due to a population of about 0.3 in the spin-down level of QD2. Contrary to the parallel configuration set up, the  $z$  component  $S_{2,el}^z$  is negative when the read-out phase starts and does not change sign [see Fig. 11(d)].

The spin current  $I_{\text{spin}}(t) \equiv I_{R,\downarrow}(t) - I_{R,\uparrow}(t)$  during the read-out phase ( $t > 60$ ) is displayed in the inset of Fig. 12 for the parallel and antiparallel configurations analyzed in Figs. 10 and 11. One observes an exponential decay with superimposed oscillations of frequency  $|\varepsilon_F + U_R \pm J_2| = 0.05$  as expected. However, a closer inspection reveals a richer structure. In Fig. 12 we show the discrete Fourier transform of  $I_{\text{spin}}(t)$  with  $t$  in the range of (65, 640). Besides the peak at  $\omega = 0.05$ , there exist an extra peak at frequency  $\omega = |2 - \varepsilon_F| \sim 2.96$  and an asymmetric peak structure at frequency  $\omega = |\varepsilon_F + 2| \sim 1.04$ . The extra transient frequencies are due to the finite bandwidth of the leads since the energies  $+2$  and  $-2$  (in units of  $V$ ) correspond the top and the bottom of the right band, respectively.

In conclusion, we have shown how to propagate in time a spinful open quantum system subjected to arbitrary time- and spin-dependent perturbations. The semi-infinite nature of the leads has been exactly accounted for. Full simulations of the microscopic charge and spin transient dynamics of a double quantum dot in its operating regime have been presented. Figure 13 summarizes how the device works by displaying the spin currents at the left and right interfaces during the entire sequence of voltage pulses. Different processing of the injected spin-up current results in different spin currents at the right interface.

## V. SUMMARY AND OUTLOOK

In the last few years we have witnessed an increasing interest on transient responses in quantum transport mainly due to their potential relevancy in molecular electronics, a field where molecular devices will possibly operate under nonsteady-state conditions. The main difficulty in the study of the short-time response of open quantum systems stems

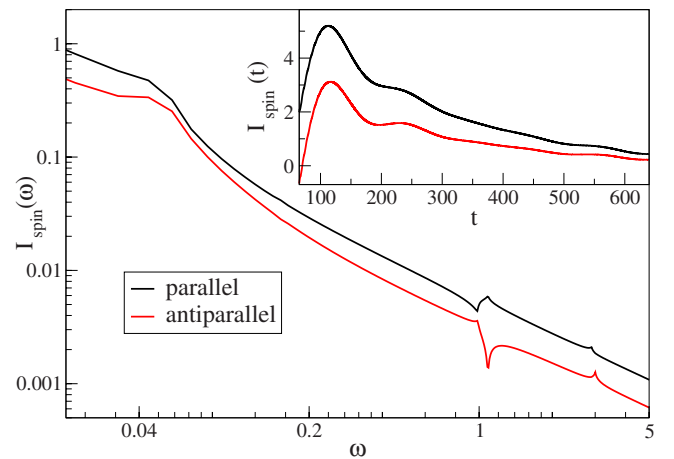


FIG. 12. (Color online) Discrete Fourier transform of the spin current  $I_{\text{spin}} = I_{R,\downarrow} - I_{R,\uparrow}$  at the right interface for the parallel and antiparallel configurations of Fig. 10 and Fig. 11, respectively. The inset shows  $I_{\text{spin}}$  in time domain with  $t$  in the range of (65, 640), which has been used to perform the discrete Fourier transform. Both  $I_{\text{spin}}(\omega)$  and  $I_{\text{spin}}(t)$  are in units of  $10^{-3}$ .

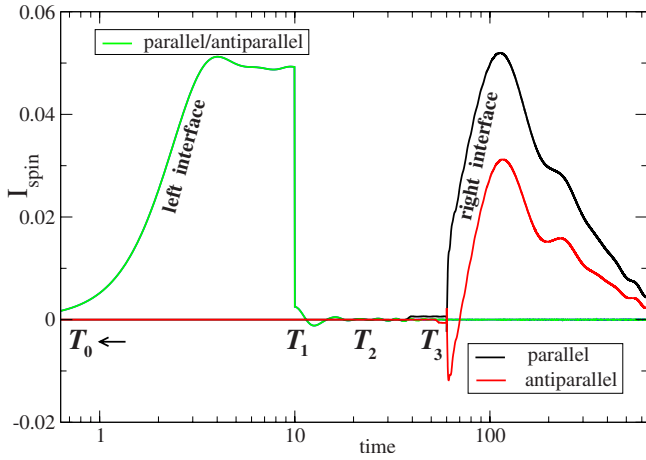


FIG. 13. (Color online) Spin current at the left and right interfaces for the parallel and antiparallel configurations of Fig. 10 and Fig. 11, respectively. For the parallel configuration  $T_0=0$ ,  $T_1=10.0$ ,  $T_2=36.5$ , and  $T_3=39.32$ , while for the antiparallel configuration  $T_0=0$ ,  $T_1=10.0$ ,  $T_2=52.05$ , and  $T_3=54.84$ .

from the macroscopic size of the leads. Several approaches have been proposed to tackle this problem. Treating the leads in the WBL approximation allows for obtaining a simple integral equation for currents, densities, etc.,<sup>37–40</sup> but lacks retardation effects. One-dimensional leads have been approximately treated within a Wigner-function approach<sup>41,42</sup> or by including only a finite number of lead unit cells.<sup>43–45</sup> Only recently it became possible to deal with the semi-infinite nature of the leads using a scheme based on wavefunction propagation<sup>30</sup> or, alternatively, other algorithms based on solving the Dyson-Keldysh equations in the time domain.<sup>46–50</sup> Few attempts to include electron-correlation<sup>51,52</sup> as well as electron-nuclear interactions<sup>53,54</sup> in the transient regime have also been made.

In this work we have used a modified version of the propagation algorithm of Ref. 30 (see Appendix B) and generalized it to include the spin degrees of freedom. We have proposed a double quantum dot system to manipulate the charge and the spin of the electrons. Numerical simulations of the entire operating regime have been provided. These include some of the crucial steps in the theory of quantum computation, e.g., the injection of spins and their readout.

The transient electron dynamics when a device is perturbed by ultrafast voltage pulses is not only relevant to our microscopic understanding but an exploitable feature to improve the device performance. This has been explicitly shown in Sec. IV: the efficiency of the spin injection can be much higher during the transient than at the steady state. We also have found that for a given height of the barriers between lead  $L$  and QD1, QD1 and QD2, and QD2 and lead  $R$ , the damping of the spin magnitude during the rotation phase is much smaller for different exchange couplings, i.e.,  $J_1 \neq J_2$ , than for  $J_1=J_2$ . This means that the spin relaxation can be substantially delayed using different quantum dots.

Using the nonequilibrium Green's function formalism in the WBL approximation, we have obtained a rate equation for both the spin-injection and spin read-out processes. For short times the rate equation becomes remarkably transparent

and permits us to identify the mechanisms leading to a relaxation of the spin magnitude and to a deterioration of the spin polarization. Going beyond the WBL approximation results in a richer structure of the transient responses as transitions between the Fermi energy and the bottom/top of the band occur as well.

As shown in Sec. IV, the possibility of simulating operational sequences, e.g., that of Fig. 1, allows for a real-time study of fundamental processes not accessible otherwise. Much more work is, however, needed before a systematic comparison with experimental data can be made. Accounting for intradot and possibly interdot electron-electron interactions is of crucial importance for describing, e.g., the Coulomb blockade or the Kondo regimes. The complications here stem from the necessity of including electron correlations in a time-dependent conserving manner, a progress which can be made either within the framework of many-body theory<sup>55</sup> or within one-particle frameworks, e.g., time-dependent density-functional theory (TDDFT).<sup>56–58</sup> Developments in the former direction have been made in steady-state situations by treating the correlation at the GW level.<sup>59–62</sup>

Another fundamental issue to be pursued is the extension to three-dimensional leads. This would allow for a proper treatment of the long-range Coulomb potential as well as for a realistic description of the atomistic structure of the tunneling barriers.

Finally, the recent experimental advances in attaching quantum dots to superconducting leads<sup>63</sup> prompt for a generalization of the propagation algorithm to leads described by, e.g., BCS-type models. Such development will give us access to a completely new phenomenology due to the competition between the pairing interaction and the spin-flip interactions, a topic not yet explored in the transient regime.

## ACKNOWLEDGMENTS

We would like to acknowledge useful discussions with S. Kurth. This work was supported in part by the EU Network of Excellence NANOQUANTA (Grant No. NMP4-CT-2004–500198). E.P. is also financially supported by Fondazione Cariplo n. Prot. 0018524.

## APPENDIX A: PROOF OF EQ. (24)

The result in Eq. (24) is a consequence of the relative orientation of the spin impurity  $\vec{S}_1$  with respect to  $\vec{S}_2$ . By definition the quantity  $[\Sigma_2^z(t)]_{1,1}$  is the (1,1) matrix element of the product of three matrices

$$[\Sigma_2^z(t)]_{1,1} = \left[ e^{-it} \begin{pmatrix} J_1 \sigma_x & V_{\text{QD}12} \\ V_{\text{QD}12} & J_2 \sigma_z \end{pmatrix} \begin{pmatrix} \mathbf{0}_2 & \mathbf{0}_2 \\ \mathbf{0}_2 & \sigma_z \end{pmatrix} e^{it} \begin{pmatrix} J_1 \sigma_x & V_{\text{QD}12} \\ V_{\text{QD}12} & J_2 \sigma_z \end{pmatrix} \right]_{1,1}. \quad (\text{A1})$$

Consider the unitary operator  $U = U_g U_z U_x$  which consists of a rotation of both spin impurities around the  $x$  axis by an angle  $\pi$ ,

$$U_x = \begin{pmatrix} \exp[-i\pi\sigma_x/2] & \mathbf{0}_2 \\ \mathbf{0}_2 & \exp[-i\pi\sigma_x/2] \end{pmatrix},$$

followed by a rotation around the  $z$  axis by an angle  $\pi$ ,

$$U_z = \begin{pmatrix} \exp[-i\pi\sigma_z/2] & \mathbf{0}_2 \\ \mathbf{0}_2 & \exp[-i\pi\sigma_z/2] \end{pmatrix},$$

and followed by a gauge transformation which changes the sign of the fermion operators on QD2,

$$U_g = \begin{pmatrix} \mathbf{1}_2 & \mathbf{0}_2 \\ \mathbf{0}_2 & -\mathbf{1}_2 \end{pmatrix}.$$

Insertions of the identity matrix  $U^\dagger U$  in Eq. (A1) gives

$$\begin{aligned} [\Sigma_2^z(t)]_{1,1} &= \left[ U^\dagger U e^{-it} \begin{pmatrix} J_1\sigma_x & V_{\text{QD}12} \\ V_{\text{QD}12} & J_2\sigma_z \end{pmatrix} U^\dagger U \begin{pmatrix} \mathbf{0}_2 & \mathbf{0}_2 \\ \mathbf{0}_2 & \sigma_z \end{pmatrix} \right. \\ &\quad \left. \times U^\dagger U e^{it} \begin{pmatrix} J_1\sigma_x & V_{\text{QD}12} \\ V_{\text{QD}12} & J_2\sigma_z \end{pmatrix} U^\dagger U \right]_{1,1} \\ &= - \left[ e^{it} \begin{pmatrix} J_1\sigma_x & V_{\text{QD}12} \\ V_{\text{QD}12} & J_2\sigma_z \end{pmatrix} \right. \\ &\quad \left. \times \begin{pmatrix} \mathbf{0}_2 & \mathbf{0}_2 \\ \mathbf{0}_2 & \sigma_z \end{pmatrix} e^{-it} \begin{pmatrix} J_1\sigma_x & V_{\text{QD}12} \\ V_{\text{QD}12} & J_2\sigma_z \end{pmatrix} \right]_{2,2} \\ &= - [\Sigma_2^z(-t)]_{2,2}. \end{aligned} \quad (\text{A2})$$

Taking into account that  $[\Sigma_2^z(t)]_{1,1}$ ,  $[\Sigma_2^z(t)]_{2,2}$  are even functions of  $t$ , Eq. (24) follows.

## APPENDIX B: PROPAGATION ALGORITHM

Let  $\mathbf{H}(t) = \sum_\alpha \mathbf{H}_\alpha(t) + \sum_\alpha (\mathbf{H}_{\alpha C}^0 + \mathbf{H}_{C\alpha}^0) + \mathbf{H}_C(t)$  be the one-particle Hamiltonian of a system which consists of  $\alpha = 1, 2, \dots, N$  electrodes in contact with a central region  $C$ . We assume that the time dependence of

$$\mathbf{H}_\alpha(t) = \begin{pmatrix} \mathbf{H}_{\alpha,\uparrow}^0 & \mathbf{0} \\ \mathbf{0} & \mathbf{H}_{\alpha,\downarrow}^0 \end{pmatrix} + \begin{pmatrix} U_{\alpha,\uparrow}(t) & \mathbf{0} \\ \mathbf{0} & U_{\alpha,\downarrow}(t) \end{pmatrix} = \mathbf{H}_\alpha^0 + \mathbf{U}_\alpha(t) \quad (\text{B1})$$

is a uniform spin-dependent and time-dependent shift while the time dependence of  $\mathbf{H}_C$  has no restrictions. We denote with  $|\psi_\alpha\rangle$  the projection of a generic wave function  $|\psi\rangle$  on electrode  $\alpha$  and with  $|\psi_C\rangle$  the projection of  $|\psi\rangle$  onto region  $C$ . The time-dependent Schrödinger equation reads

$$i \frac{d}{dt} |\psi_\alpha(t)\rangle = \mathbf{H}_\alpha(t) |\psi_\alpha(t)\rangle + \mathbf{H}_{\alpha C}^0 |\psi_C(t)\rangle, \quad (\text{B2})$$

$$i \frac{d}{dt} |\psi_C(t)\rangle = \mathbf{H}_C(t) |\psi_C(t)\rangle + \sum_\alpha \mathbf{H}_{C\alpha}^0 |\psi_\alpha(t)\rangle. \quad (\text{B3})$$

Performing the gauge transformation

$$|\psi_\alpha(t)\rangle = \exp \left[ -i \int_0^t d\tau U_\alpha(\tau) \right] |\phi_\alpha(t)\rangle, \quad (\text{B4})$$

and  $|\psi_C(t)\rangle = |\phi_C(t)\rangle$ , Eqs. (B2) and (B3) become

$$i \frac{d}{dt} |\phi_\alpha(t)\rangle = \mathbf{H}_\alpha^0 |\psi_\alpha(t)\rangle + \mathbf{H}_{\alpha C}(t) |\phi_C(t)\rangle, \quad (\text{B5})$$

$$i \frac{d}{dt} |\phi_C(t)\rangle = \mathbf{H}_C(t) |\phi_C(t)\rangle + \sum_\alpha \mathbf{H}_{C\alpha}(t) |\phi_\alpha(t)\rangle, \quad (\text{B6})$$

with  $\mathbf{H}_{C\alpha}(t) = \mathbf{H}_{C\alpha}^0 \exp[-i \int_0^t d\tau U_\alpha(\tau)]$  and  $\mathbf{H}_{\alpha C}(t) = [\mathbf{H}_{C\alpha}(t)]^\dagger$ . The effect of the gauge transformation is to transfer the time dependence from the Hamiltonian describing the bulk electrodes to the Hamiltonian describing the contacts between the electrodes and region  $C$ . The gauge-transformed Schrödinger equation is used to calculate the time-evolved state  $|\phi(t_m = m\Delta t)\rangle \equiv |\phi^{(m)}\rangle$  by using the Cayley method

$$(1 + i\delta \mathbf{H}_g^{(m)}) |\phi^{(m+1)}\rangle = (1 - i\delta \mathbf{H}_g^{(m)}) |\phi^{(m)}\rangle, \quad (\text{B7})$$

where  $\delta = \Delta t/2$ ,  $\mathbf{H}_g^{(m)} = \frac{1}{2} [\mathbf{H}_g(t_{m+1}) + \mathbf{H}_g(t_m)]$ , and  $\mathbf{H}_g(t) = \sum_\alpha \mathbf{H}_\alpha^0 + \sum_\alpha [\mathbf{H}_{\alpha C}(t) + \mathbf{H}_{C\alpha}(t)] + \mathbf{H}_C(t)$  is the gauge-transformed Hamiltonian. The interface Hamiltonian  $\mathbf{H}_{\alpha C}$  is spin diagonal provided that region  $C$  includes the first few atomic layers of electrode  $\alpha$ . In this case the projection of Eq. (B7) onto different subregions leads to a close recursive relation for the amplitudes  $|\phi_C^{(m)}\rangle$  of the wave function in region  $C$  (the steps are similar to those of Ref. 30),

$$|\phi_C^{(m+1)}\rangle = \frac{1 - i\delta \mathbf{H}_{\text{eff}}^{(m)}}{1 + i\delta \mathbf{H}_{\text{eff}}^{(m)}} |\phi_C^{(m)}\rangle + |S^{(m)}\rangle - |M^{(m)}\rangle, \quad (\text{B8})$$

where the source term  $|S^{(m)}\rangle$  and the memory term  $|M^{(m)}\rangle$  read

$$|S^{(m)}\rangle = \frac{-2i\delta}{1 + i\delta \mathbf{H}_{\text{eff}}^{(m)}} \sum_\alpha \mathbf{z}_\alpha^{(m)} \mathbf{H}_{C\alpha}^0 \frac{(1 - i\delta \mathbf{H}_\alpha^0)^m}{(1 + i\delta \mathbf{H}_\alpha^0)^{m+1}} |\phi_\alpha^{(0)}\rangle, \quad (\text{B9})$$

$$\begin{aligned} |M^{(m)}\rangle &= \frac{\delta^2}{1 + i\delta \mathbf{H}_{\text{eff}}^{(m)}} \sum_{\alpha} \sum_{j=0}^{m-1} \mathbf{z}_\alpha^{(m)} (\mathbf{Q}_\alpha^{(j)} + \mathbf{Q}_\alpha^{(j+1)}) \\ &\quad \times \bar{\mathbf{z}}_\alpha^{(m-1-j)} (|\phi_C^{(m-j)}\rangle + |\phi_C^{(m-1-j)}\rangle). \end{aligned} \quad (\text{B10})$$

In the above equations we have used the following definitions:

$$\mathbf{z}_\alpha^{(m)} = \frac{\exp \left[ -i \int_0^{t_{m+1}} d\tau U_\alpha(\tau) \right] + \exp \left[ -i \int_0^{t_m} d\tau U_\alpha(\tau) \right]}{2}, \quad (\text{B11})$$

$$\mathbf{Q}_\alpha^{(m)} = \mathbf{H}_{C\alpha}^0 \frac{(1 - i\delta \mathbf{H}_\alpha^0)^m}{(1 + i\delta \mathbf{H}_\alpha^0)^{m+1}} \mathbf{H}_{\alpha C}^0, \quad (\text{B12})$$

$$\mathbf{H}_{\text{eff}}^{(m)} = \mathbf{H}_C^{(m)} - i\delta \sum_\alpha \mathbf{z}_\alpha^{(m)} \mathbf{Q}_\alpha^{(0)} \bar{\mathbf{z}}_\alpha^{(m)}. \quad (\text{B13})$$

The recursive relation in Eq. (B8) is written in terms of matrices and vectors with the same dimension of the central region, i.e., the infinitely large electrodes have been embedded in an effective equation of finite dimension. We defer the reader to Ref. 30 for the description of how to calculate the matrices  $\mathbf{Q}_\alpha^{(m)}$  and the source term  $|S^{(m)}\rangle$ .

\*gianluca.stefanucci@roma2.infn.it

- <sup>1</sup>M. A. Nielsen and I. L. Chuang, *Quantum Computation and Quantum Information* (Cambridge University Press, Cambridge, England, 2000).
- <sup>2</sup>D. Awschalom, N. Samarth, and D. Loss, *Semiconductor Spintronics and Quantum Computation* (Springer, Berlin, 2002).
- <sup>3</sup>R. Hanson, L. P. Kouwenhoven, J. R. Petta, S. Tarucha, and L. M. K. Vandersypen, *Rev. Mod. Phys.* **79**, 1217 (2007).
- <sup>4</sup>D. Loss and D. P. DiVincenzo, *Phys. Rev. A* **57**, 120 (1998).
- <sup>5</sup>*Spin-Dependent Transport in Magnetic Nanostructures*, edited by S. Maekawa and T. Shinjo (Taylor & Francis, London, 2002).
- <sup>6</sup>S. Moskal, S. Bednarek, and J. Adamowski, *Phys. Rev. A* **71**, 062327 (2005).
- <sup>7</sup>T. Fujisawa, T. Hayashi, and S. Sasaki, *Rep. Prog. Phys.* **69**, 759 (2006).
- <sup>8</sup>F. M. Souza, S. A. Leao, R. M. Gester, and A. P. Jauho, *Phys. Rev. B* **76**, 125318 (2007).
- <sup>9</sup>F. M. Souza, *Phys. Rev. B* **76**, 205315 (2007).
- <sup>10</sup>J. Fransson, *Phys. Rev. B* **77**, 205316 (2008).
- <sup>11</sup>J. Fransson, *Nanotechnology* **19**, 285714 (2008).
- <sup>12</sup>T. Hayashi, T. Fujisawa, H. D. Cheong, Y. H. Jeong, and Y. Hirayama, *Phys. Rev. Lett.* **91**, 226804 (2003).
- <sup>13</sup>R. Hanson, B. Witkamp, L. M. K. Vandersypen, L. H. Willems van Beveren, J. M. Elzerman, and L. P. Kouwenhoven, *Phys. Rev. Lett.* **91**, 196802 (2003).
- <sup>14</sup>J. M. Elzerman, R. Hanson, L. H. Willems van Beveren, B. Witkamp, L. M. K. Vandersypen, and L. P. Kouwenhoven, *Nature (London)* **430**, 431 (2004).
- <sup>15</sup>R. Hanson, L. H. Willems van Beveren, I. T. Vink, J. M. Elzerman, W. J. M. Naber, F. H. L. Koppens, L. P. Kouwenhoven, and L. M. K. Vandersypen, *Phys. Rev. Lett.* **94**, 196802 (2005).
- <sup>16</sup>J. R. Petta, A. C. Johnson, J. M. Taylor, E. A. Laird, A. Yacoby, M. D. Lukin, C. M. Marcus, M. P. Hanson, and A. C. Gossard, *Science* **309**, 2180 (2005).
- <sup>17</sup>F. H. L. Koppens, C. Buizert, K. J. Tielrooij, I. T. Vink, K. C. Nowack, T. Meunier, L. P. Kouwenhoven, and L. M. K. Vandersypen, *Nature (London)* **442**, 766 (2006).
- <sup>18</sup>M. Kataoka, R. J. Schneble, A. L. Thorn, C. H. W. Barnes, C. J. B. Ford, D. Anderson, G. A. C. Jones, I. Farrer, D. A. Ritchie, and M. Pepper, *Phys. Rev. Lett.* **98**, 046801 (2007).
- <sup>19</sup>Y. Manassen, R. J. Hamers, J. E. Demuth, and A. J. Castellano, Jr., *Phys. Rev. Lett.* **62**, 2531 (1989).
- <sup>20</sup>Y. Manassen, I. Mukhopadhyay, and N. R. Rao, *Phys. Rev. B* **61**, 16223 (2000).
- <sup>21</sup>W. A. Coish and D. Loss, *Phys. Rev. B* **75**, 161302(R) (2007).
- <sup>22</sup>A. V. Kimel, A. Kirilyuk, and T. Rasing, *Laser Photonics Rev.* **1**, 275 (2007).
- <sup>23</sup>Jian-Xin Zhu and A. V. Balatsky, *Phys. Rev. Lett.* **89**, 286802 (2002).
- <sup>24</sup>H.-Q. Zhou and S. Y. Cho, *J. Phys.: Condens. Matter* **17**, 7433 (2005).
- <sup>25</sup>S. K. Joshi, D. Sahoo, and A. M. Jayannavar, *Phys. Rev. B* **64**, 075320 (2001).
- <sup>26</sup>A. Aldea, M. Tolea, and J. Zittartz, *Physica E (Amsterdam)* **28**, 191 (2005).
- <sup>27</sup>F. Ciccarello, G. M. Palma, and M. Zarcone, *Phys. Rev. B* **75**, 205415 (2007).
- <sup>28</sup>F. Ciccarello, G. M. Palma, M. Zarcone, Y. Omar, and V. R. Vieira, *New J. Phys.* **8**, 214 (2006).
- <sup>29</sup>F. Ciccarello, G. M. Palma, M. Zarcone, Y. Omar, and V. R. Vieira, *J. Phys. A: Math. Theor.* **40**, 7993 (2007).
- <sup>30</sup>S. Kurth, G. Stefanucci, C.-O. Almbladh, A. Rubio, and E. K. U. Gross, *Phys. Rev. B* **72**, 035308 (2005).
- <sup>31</sup>M. Cini, *Phys. Rev. B* **22**, 5887 (1980).
- <sup>32</sup>H.-Z. Lu and S.-Q. Shen, *Phys. Rev. B* **77**, 235309 (2008).
- <sup>33</sup>G. Stefanucci and C.-O. Almbladh, *Phys. Rev. B* **69**, 195318 (2004).
- <sup>34</sup>J. A. Gupta, R. Knobel, N. Samarth, and D. D. Awschalom, *Science* **292**, 2458 (2001).
- <sup>35</sup>R. C. Myers, K. C. Ku, X. Li, N. Samarth, and D. D. Awschalom, *Phys. Rev. B* **72**, 041302(R) (2005).
- <sup>36</sup>The weak link  $V^{(3)}=0.05$  between QD2 and lead  $R$  yields two sharp resonances at  $\pm J_2$  in the local density of states of QD2. Tuning the electrochemical potential  $\mu_R=\epsilon_F+U_R$  in between the resonances the spin current is larger as compared to the case  $\mu_R < -J_2$  or  $\mu_R > J_2$ .
- <sup>37</sup>A.-P. Jauho, N. S. Wingreen, and Y. Meir, *Phys. Rev. B* **50**, 5528 (1994).
- <sup>38</sup>Q.-f. Sun and T.-h. Lin, *J. Phys.: Condens. Matter* **9**, 3043 (1997).
- <sup>39</sup>J. Q. You, C.-H. Lam, and H. Z. Zheng, *Phys. Rev. B* **62**, 1978 (2000).
- <sup>40</sup>X. Zheng, F. Wang, C. Y. Yam, Y. Mo, and G. H. Chen, *Phys. Rev. B* **75**, 195127 (2007).
- <sup>41</sup>W. R. Frensley, *Rev. Mod. Phys.* **62**, 745 (1990).
- <sup>42</sup>Z. Dai and J. Ni, *Phys. Lett. A* **342**, 272 (2005).
- <sup>43</sup>N. Bushong, N. Sai, and M. Di Ventra, *Nano Lett.* **5**, 2569 (2005).
- <sup>44</sup>A. Dhar and D. Sen, *Phys. Rev. B* **73**, 085119 (2006).
- <sup>45</sup>A. Agarwal and D. Sen, *J. Phys.: Condens. Matter* **19**, 046205 (2007).
- <sup>46</sup>Y. Zhu, J. Maciejko, T. Ji, H. Guo, and J. Wang, *Phys. Rev. B* **71**, 075317 (2005).
- <sup>47</sup>D. Hou, Y. He, X. Liu, J. Kang, J. Chen, and R. Han, *Physica E (Amsterdam)* **31**, 191 (2006).
- <sup>48</sup>J. Maciejko, J. Wang, and H. Guo, *Phys. Rev. B* **74**, 085324 (2006).
- <sup>49</sup>Y. He, D. Hou, X. Liu, R. Han, and J. Chen, *IEEE Trans. Nanotechnol.* **6**, 56 (2007).
- <sup>50</sup>V. Moldoveanu, V. Gudmundsson, and A. Manolescu, *Phys. Rev. B* **76**, 085330 (2007).
- <sup>51</sup>Q.-f. Sun and T.-h. Lin, *J. Phys.: Condens. Matter* **9**, 4875 (1997).
- <sup>52</sup>T. Kwapinski, R. Taranko, and E. Taranko, *Acta Phys. Pol. A* **99**, 293 (2001).
- <sup>53</sup>C. Verdozzi, G. Stefanucci, and C.-O. Almbladh, *Phys. Rev. Lett.* **97**, 046603 (2006).
- <sup>54</sup>C. G. Sanchez, M. Stamenova, S. Sanvito, D. R. Bowler, A. P. Horsfield, and T. N. Todorov, *J. Chem. Phys.* **124**, 214708 (2006).
- <sup>55</sup>G. Baym, *Phys. Rev.* **127**, 1391 (1962).
- <sup>56</sup>E. Runge and E. K. U. Gross, *Phys. Rev. Lett.* **52**, 997 (1984).
- <sup>57</sup>U. von Barth, N. E. Dahlen, R. van Leeuwen, and G. Stefanucci, *Phys. Rev. B* **72**, 235109 (2005).
- <sup>58</sup>We here wish to mention that the use of TDDFT in lattice models is, at the moment, not rigorously founded as there is no proof that an interacting time-dependent density can be reproduced in a system of noninteracting electrons. This issue has been recently discussed by R. Baer, *J. Chem. Phys.* **128**, 044103 (2008); C. Verdozzi, arXiv:0707.2317 (unpublished); Y. Li and

- C. A. Ullrich, *J. Chem. Phys.* **129**, 044105 (2008).
- <sup>59</sup>K. S. Thygesen and A. Rubio, *J. Chem. Phys.* **126**, 091101 (2007).
- <sup>60</sup>P. Darancet, A. Ferretti, D. Mayou, and V. Olevano, *Phys. Rev. B* **75**, 075102 (2007).
- <sup>61</sup>X. Wang, C. D. Spataru, M. S. Hybertsen, and A. J. Millis, *Phys. Rev. B* **77**, 045119 (2008).
- <sup>62</sup>K. S. Thygesen and A. Rubio, *Phys. Rev. B* **77**, 115333 (2008).
- <sup>63</sup>C. Buizert, A. Oiwa, K. Shibata, K. Hirakawa, and S. Tarucha, *Phys. Rev. Lett.* **99**, 136806 (2007).